New Phytologist

Research

Ethylene signaling regulates natural variation in the abundance of antifungal acetylated diferuloylsucroses and *Fusarium graminearum* resistance in maize seedling roots

Shaoqun Zhou[1,2], Ying K. Zhang[1,3], Karl A. Kremling[4], Yezhang Ding[5], John S. Bennett[6], Justin S. Bae[1], Dean K. Kim[1], Hayley H. Ackerman[1], Michael V. Kolomiets[6], Eric A. Schmelz[5], Frank C. Schroeder[1], Edward S. Buckler[4,7] and Georg Jander[1]

[1]Boyce Thompson Institute, 533 Tower Road, Ithaca, NY 14853, USA; [2]Plant Biology Section, School of Integrated Plant Science, Cornell University, Ithaca, NY 14853, USA; [3]Department of Chemistry and Chemical Biology, Cornell University, Ithaca, NY 14853, USA; [4]Plant Breeding and Genetics Section, Cornell University, Ithaca, NY 14853, USA; [5]Section of Cell and Developmental Biology, University of California at San Diego, La Jolla, CA 92093, USA; [6]Department of Plant Pathology and Microbiology, Texas A&M University, College Station, TX 77840, USA; [7]United States Department of Agriculture-Agricultural Research Service, Robert W. Holley Center for Agriculture and Health, Ithaca, NY 14853, USA

Author for correspondence:
Georg Jander
Tel: +1 607 254 1365
Email: gj32@cornell.edu

Received: *6 May 2018*
Accepted: *26 September 2018*

New Phytologist (2018)
doi: 10.1111/nph.15520

Key words: acetylated diferuloylsucrose, ethylene, *Fusarium graminearum*, metabolite quantitative trait locus (QTL) mapping, *Zea mays* (maize).

Summary

- The production and regulation of defensive specialized metabolites play a central role in pathogen resistance in maize (*Zea mays*) and other plants. Therefore, identification of genes involved in plant specialized metabolism can contribute to improved disease resistance.
- We used comparative metabolomics to identify previously unknown antifungal metabolites in maize seedling roots, and investigated the genetic and physiological mechanisms underlying their natural variation using quantitative trait locus mapping and comparative transcriptomics approaches.
- Two maize metabolites, smilaside A (3,6-diferuloyl-3′,6′-diacetylsucrose) and smiglaside C (3,6-diferuloyl-2′,3′,6′-triacetylsucrose), were identified that could contribute to maize resistance against *Fusarium graminearum* and other fungal pathogens. Elevated expression of an ethylene signaling gene, *ETHYLENE INSENSITIVE 2* (*ZmEIN2*), co-segregated with a decreased smilaside A : smiglaside C ratio. Pharmacological and genetic manipulation of ethylene availability and sensitivity *in vivo* indicated that, whereas ethylene was required for the production of both metabolites, the smilaside A : smiglaside C ratio was negatively regulated by ethylene sensitivity. This ratio, rather than the absolute abundance of these two metabolites, was important for maize seedling root defense against *F. graminearum*.
- Ethylene signaling regulates the relative abundance of the two *F. graminearum*-resistance-related metabolites and affects resistance against *F. graminearum* in maize seedling roots.

Introduction

Plants in natural and man-made ecosystems are continuously exposed to microbial pathogens. Specialized metabolic pathways that give rise to diverse arsenals of bioactive defense compounds allow plants to fend off pathogen attacks. The significance of plant specialized metabolism in agriculture is exemplified by the association of specific biosynthetic genes with resistance against insect pests and phytopathogens (Meihls *et al.*, 2013; Handrick *et al.*, 2016; Yang *et al.*, 2017). Such studies highlight the potential of enlisting naturally occurring specialized metabolites in crop species to enhance quantitative disease resistance.

In North America, maize (*Zea mays*) is the most important agricultural crop, with over 13 billion bushels produced per annum, of which *c.* 10% is lost to disease (Mueller, 2016a,b, 2017). Maize also is known for its great genetic diversity, involving both nucleotide polymorphisms and structural genomic variation (Buckler *et al.*, 2006; Jiao *et al.*, 2017). The genetic architecture of disease resistance in maize has been investigated extensively using publicly available genetic resources (Mideros *et al.*, 2012; Olukolu *et al.*, 2014; Benson *et al.*, 2015). Compared to foliar and ear diseases, maize seedling diseases remain a relatively understudied area, even though in some years they can account for more yield loss than any single disease in the aboveground tissues (Mueller, 2016a). This may be because experimental methods developed for large-scale screening of diseases in aboveground tissues, such as controlled pathogen inoculation and visual symptom scoring, are difficult to apply to seedling diseases under field conditions.

Fusarium graminearum is one of the most common causal pathogens of maize seedling disease in the northern temperate zone. In the field, it overwinters on crop residue as thickened

hyphae and produces asexual conidia that infect germinating seedlings roots or mesocotyls. Depending on the developmental stage and infection site, *F. graminearum* also can cause root rot, stem rot and ear rot in maize (Munkvold & White, 2016). Previous research on maize–*F. graminearum* interactions has focused primarily on ear rot, with results generally showing that resistance against this disease is controlled by numerous small-effect quantitative trait loci (QTL) that are influenced by experimental methods and genetic backgrounds (Ali *et al.*, 2005; Kebede *et al.*, 2016; Brauner *et al.*, 2017). Furthermore, transcriptomic studies in maize and wheat show that host–*F. graminearum* interactions are significantly influenced by host tissue types, suggesting that the QTL associated with *F. graminearum* ear rot resistance probably will not confer resistance in seedling roots (Kazan *et al.*, 2012; Zhang *et al.*, 2016).

Compared to QTL identified from *F. graminearum* ear rot studies, factors contributing to *F. graminearum* stalk rot resistance may be more relevant to infections of seedling roots. For instance, near-isogenic lines (NILs) selected based on stalk rot resistance phenotypes also showed significant differences in primary root symptoms after controlled inoculation (Ye *et al.*, 2013). *Fusarium graminearum* infection in maize stalks induces production of specialized metabolites with antifungal activities (Huffaker *et al.*, 2011; Schmelz *et al.*, 2011). Additionally, comparative and correlative studies have identified constitutive phytoanticipins that were associated with *F. graminearum* resistance. For example, an *F. graminearum*-resistant NIL was found to accumulate significantly higher content of phenolic acids in its seedling roots compared to its susceptible relative. Interestingly, these differences disappear after *F. graminearum* infection, primarily due to fungus-induced reduction of defenses in the resistant NILs (Ye *et al.*, 2013). The same compounds also have been identified as metabolites related to *F. graminearum* resistance in other crop species, and were shown to inhibit fungal growth *in vitro* (Bollina *et al.*, 2010; Ponts *et al.*, 2011). Taken together, these studies indicate that specialized metabolites in maize seedling roots play a significant role in resistance against *F. graminearum.*

In the present paper we describe a comparative metabolomics approach using maize inbred lines B73 and Mo17 to identify previously unknown maize antifungal compounds. These experiments led to the identification of two acetylated diferuloylsucroses, one of which demonstrated significant fungal growth inhibition *in vitro* at a physiologically relevant concentration. Genetic mapping, analysis of mutants and physiological experiments demonstrated that accumulation of acetylated diferuloylsucroses is promoted by ethylene production and fine-tuned by ethylene sensitivity in maize.

Materials and Methods

Plant growth and fungal inoculation

All maize lines were obtained from the Maize Genetics Cooperation Stock Center (Urbana Champaign, IL, USA). Seedling germination and fungal inoculation were carried out as described previously (Zhou *et al.*, 2018). All seedling inoculation experiments involved *Fusarium graminearum* strain ZTE, which was obtained from Dr Frances Trail (Guenther & Trail, 2005) and is derived from a field-collected strain Z-3639 (Proctor *et al.*, 1995) transformed with the plasmid pTEFEGFP (Vanden Wymelenberg *et al.*, 1997), with permission from Dr Robert Proctor. Six days after inoculation, the total root length of seedlings was measured with the RootReader 2D system (Famoso *et al.*, 2010). For screening of natural variation in *F. graminearum*-induced morphological changes, at least five seedlings of each plant line were mock- or fungus-inoculated in two independent experiments for root length measurement. In two other experiments, seven B73 and Mo17 seedlings were inoculated and measured as described above, and their root tissue was harvested for further analysis.

Fusarium graminearum gene expression measurement, mycotoxin quantification, visual symptom scoring and ergosterol assay

The expression of the *F. graminearum* β-tubulin gene in seedling roots was measured using a previously published protocol (Lou *et al.*, 2016). The primers used for quantitative reverse transcription polymerase chain reaction (qRT-PCR) detection of *F. graminearum* were FgTUB-qF293 (5′-ATGCTTCCAACA ACTATGCT-3′) and FgTUB-qR411 (5′-AACTAGGAAACCC TGGAGAC-3′), designed based on the *F. graminearum* strain PH-1 reference genome sequence (Cuomo *et al.*, 2007). Fungal gene expression in each replicate was normalized by measurement of the expression of a constitutive maize actin gene with the following primers ZmActin-qF (5′-CCATGAGGCCACGTAC AACT-3′) and ZmActin-qR (5′-GGTAAAACCCCACTGAG GA-3′).

Approximately 100 mg of fresh frozen seedling root tissue of each sample was used for extraction of deoxynivalenol, the main *F. graminearum* mycotoxin. Three microliters of 50 : 49.9 : 0.1, methanol : water : formic acid extraction solvent (Sigma-Aldrich) were added per mg of tissue. Ground tissue and extraction solvent were mixed and incubated at 4°C for 40 min. Solid debris was precipitated by centrifuging at 10 000 ***g*** for 10 min. For each sample, 200 µl clear extract were filtered through a 0.45-µm filter plate. Deoxynivalenol content in the extract was then measured with an Enzyme-Linked Immuno-Sorbent Assay (ELISA) kit following the manufacturer's protocol (Helica Biosystems, Santa Ana, CA, USA). Visual symptoms in seedling roots were scored 3 wk after *F. graminearum* inoculation on a 0–4 scale (0 = symptom-less; 1 = single restricted necrosis spot; 2 = single extended necrosis or multiple restricted necrosis spots; 3 = widespread necrosis throughout; 4 = seedling dead).

For ergosterol measurements, *F. graminearum*-treated seedlings were transplanted into pots of twice-autoclaved TX360 Metro Mix and grown for 3 wk. Ergosterol was analyzed as described previously (Christensen *et al.*, 2014), with the following modifications: roots were crushed and placed in scintillation vials each with 10 ml of chloroform:methanol (2 : 1, v/v) (99.8%) followed by incubation in darkness overnight at room temperature. One milliliter of extract from each vial was syringe-filtered through

0.45-μm cellulose acetate membrane filters, and 50 μl of filtrate was added to 50 μl of 10 μM ^{13}C-labeled cholesterol (cholesterol-25,26,27–^{13}C; Sigma) in methanol as internal standard. Ergosterol was quantified using an Ascentis Express C-18 column (3 cm × 2.1 mm, 2.7 μm) connected to an API 3200 LC/MS/MS with atmospheric photochemical ionization. The injection volume was 5 μl and the isocratic mobile phase consisted of acetonitrile at a flow rate of 300 μl min^{-1}.

Maize root metabolomics analyses

The extraction protocol for deoxynivalenol also was used for plant-specialized metabolite extraction. Root extracts were analyzed using LC-MS. Chromatography was performed on a Dionex 3000 Ultimate UPLC-diode array detector system coupled to Thermo Q-Exactive mass spectrometer. Root extract samples were separated on a Titan C18 7.5 cm × 2.1 mm × 1.9 μm, Supelco Analytical Column (Sigma-Aldrich) with a flow rate of 0.5 ml min^{-1}, using a gradient flow of 0.1% formic acid in LC-MS grade water (eluent A) and 0.1% formic acid in acetonitrile (eluent B). Initial metabolite profiling experiments involved an 8-min linear gradient from 95:5 A:B to 0:100 A:B for comparison of *F. graminearum* induced metabolomic changes in B73 and Mo17 seedling roots. This method was extended to a 15-min gradient for better separation in later experiments. Mass spectral parameters were set as follows: spray voltage 3500 V, capillary temperature 300°C, sheath gas 35 units, auxiliary gas 10 units, probe heater temperature 200°C with a HESI probe. Full-scan mass spectra were collected (R:35000 FWHM at mass-to-charge ratio (m/z) 200; mass range: m/z 100–900) in both positive and negative electron spray ionization (ESI) modes. For nontargeted metabolomics analyses, metabolite abundance was estimated with signal intensity acquired through the XCMS-CAMERA mass scan data processing pipeline (Tautenhahn *et al.*, 2008; Benton *et al.*, 2010; Kuhl *et al.*, 2012). Smilaside A and smiglaside C abundances were estimated using peak areas at the respective m/z channel under negative ESI mode. Metabolite quantification was normalized by the total ion concentration, dividing each mass feature intensity by the sum of all mass feature intensities within each sample, to account for technical variation between samples. For nontargeted comparative metabolomics analyses, Student's t-tests were used to identify mass features that were constitutively different between B73 and Mo17 ($P < 0.01$, and fold-change > 2) and significantly changed by *F. graminearum* in B73 ($P < 0.01$, and fold-change > 1.5).

Structural identification of smiglaside C and smilaside A

In order to determine the chemical structures of smiglaside C and smilaside A, bulk maize seedling roots were extracted with 100% methanol at 4°C overnight. This extraction solvent, which is less polar than that used for the original LC-MS metabolite profiling experiments, was adopted to improve the extraction efficiency of the relatively nonpolar targeted compounds. Solid debris was filtered out and the crude extract was concentrated with a Buchi Rotovapor, New Castle, DE, USA. The concentrated crude extract was fractionated on a normal phase column with a methanol : dichloromethane gradient on a CombiFlash Rf+ (Teledyne Isco, Lincoln, NE, USA), and further purified for the target compounds with a water:acetonitrile gradient on a ZORBAX Eclipse XDB C18 column on an Agilent 1100 HPLC system (Agilent, Santa Clara, CA, USA). Purified compounds were dried, weighed and re-dissolved in methanol. NMR spectroscopy analyses were carried out on a Unity INOVA 600 instrument (Varian Medical Systems, Palo Alto, CA, USA) with the following conditions: 256 scan for 1H NMR; NT = 16 and NI = 800 for COSY and HSQC; NT = 32 and NI = 1600.

Determination of *in vitro* antifungal activity of smiglaside C and smilaside A

By running a standard curve with the purified compound using the same LC-MS method with incremental injection volume, the concentrations of smiglaside C to smilaside A were determined as *c.* 0.2 mM and 0.1 mM in *F. graminearum*-induced Mo17 seedling roots, respectively. Purified compounds were re-dissolved in dimethyl sulfoxide (DMSO) to 10-fold of their respective *in vivo* concentrations (i.e. 2 mM smiglaside C and 1 mM smilaside A). An *F. graminearum* spore and hyphae suspension was prepared as described above, 80 μl of it was mixed with 100 μl potato dextrose broth and 20 μl of the testing compounds in a 96-well plate; 20 μl of pure DMSO were included as the negative control for this experiment. Fungal growth was monitored by light absorbance measurement at 405 nm at 30-min intervals for 12 h at 28°C (Huffaker *et al.*, 2011). All treatment groups were measured in at least four replicates for statistical comparison.

QTL mapping of the constitutive content of smiglaside C, smilaside A and their ratio

For genetic mapping of constitutive metabolite abundance, three seedlings were germinated for 83 Intermated B73 × Mo17 (IBM) recombinant inbred lines (RIL) and five for either parental lines, B73 and Mo17 (Lee *et al.*, 2002). Ten-day-old root tissues from the three seedlings of each RIL were pooled into one sample for LC-MS analyses, whereas the five B73 and Mo17 seedlings were analyzed individually to allow comparison of their constitutive metabolomes. QTL mapping analysis was performed based on published genotype data using the composite interval mapping algorithm implemented in WinQTL Cartographer v.2.5 (Wang *et al.*, 2012).The significance thresholds of these QTL mapping results were determined with 500 permutations. For the ratio mapping, the smilaside A : smiglaside C ratio was used. Three 10-d-old seedling roots of each B73 × Mo17 near isogenic line (NIL), with reciprocal introgressions at the QTL identified with the RILs, were pooled for LC-MS analyses. Three replicates of each parental line were included as controls.

Maize root transcriptome analysis

Total RNA of 73 IBM RILs (one replicate) and the two parental lines (five replicates) were extracted with the Promega SV Total

RNA Isolation Kit from another aliquot of the same seedling root tissues used for nontargeted metabolite profiling. mRNA sequencing libraries were prepared robotically on a Biomek NXp with manual post-PCR cleanup using the Lexogen QuantSeq 3′ mRNA-Seq Library Prep Kits (Kremling *et al.*, 2018). These libraries were pooled into one lane and sequenced with 90 bp single-end reads on an Illumina NextSeq 500 with v2 chemistry at the Cornell Biotechnological Resource Center. Raw RNAseq read data were aligned to B73 RefGen_v3 5b+ gene models using the STAR v.2.5.1 RNAseq-aligner (Dobin *et al.*, 2013). The raw transcript counts were calculated for each gene model in each sample using the HTSEQ 0.6.1p2 Python module (Anders *et al.*, 2015). Finally, gene models with fewer than 10 raw read counts in any one of the 73 samples were filtered out, and raw transcript count for each gene model was normalized by the total transcript count of each sample.

1-aminocyclopropane-1-carboxylic acid (ACC) and 1-methylcyclopropene (1-MCP) treatment

Maize seedlings were grown in Turface and treated with either 100 µl of 50 mM 1-ACC solution or water control for five consecutive days starting when the seedlings emerged *c.* 2 cm above the soil line.

In a separate set of experiments, *F. graminearum*-inoculated B73 seedlings were transplanted into Turface and kept in 70-l airtight boxes. The bottoms of the boxes were filled with water and EthylBloc (0.14% 1-MCP) sachets to reach a final concentration of 5 g l^{-1} 1-MCP. Pots containing maize seedlings were elevated from water surface to avoid direct contact with the solution. 1-ACC and water control treatments were conducted using the same setup to ensure comparability with the 1-MCP treated seedlings. The predicted plant growth effects of 1-ACC and 1-MCP treatments were confirmed by measuring seedling heights in each treatment group.

In order to confirm that *F. graminearum* growth was not influenced directly by 1-ACC and 1-MCP treatment, plugs of fungal hyphae were transferred to the center of potato dextrose agar plates placed in the sealed 70-l boxes used for seedling experiments. For 1-MCP treatment, EthylBloc was used at the same concentration as described above. For 1-ACC treatment, 50 mM 1-ACC stock solution in DMSO was added to a final concentration of 50 µM. The same final concentration of DMSO was included in plates used for controls and 1-MCP treatments. Fungus radial growth was measured after 4 d.

For both 1-ACC and 1-MCP experiments, seedling roots were harvested for targeted metabolic analysis with the LC-MS method described above. To confirm that the *Zmacs2-1 Zmacs6* double mutant seedlings were producing less ethylene in their root tissues, 1 mg samples of ground frozen root tissues were placed in airtight 8-ml glass vials for ethylene collection for 29 h. One milliliter samples were injected into an Agilent Technologies 6850 Network GC system to estimate ethylene content. The ethylene peak was identified and quantified by comparing to a standard of known concentration, and normalized for tissue weight. Fungus-inoculated seedling roots were examined under an Olympus SZX-12 stereo-microscope with LP Green filter cube to compare fungus spread semi-quantitatively before frozen for LC-MS analysis. Another aliquot of these root tissues was used for qRT-PCR quantification of *F. graminearum*-specific gene expression to estimate fungal growth, as described above.

Smiglaside C and smilaside A induction by multiple fungal pathogens

Mo17 stem elicitation assays utilized 35-d-old glasshouse grown plants in 1-l pots. Plants in damage-related treatment groups were slit in the center, spanning both sides of the stem, with a surgical scalpel that was pulled 8–10 cm upward to create a parallel longitudinal incision. The damage treatments spanned the upper nodes, internodes and the most basal portion of unexpanded leaves. *Aspergillus flavus*, *Rhizopus microspores*, *Fusarium verticilloides* and *Cochliobolus heterostrophus* fungal spore inoculations were conducted with 100 µl of water per plant at a concentration of 1×10^7 spores ml^{-1} (Ding *et al.*, 2017). Damage plus water alone was used for a mock inoculation. Localized areas of control and treated stem tissues were covered with clear plastic packing tape to minimize tissue desiccation, and stem tissues were harvested 4 d later from each individual plant.

Maize stem tissues were ground to a fine powder in liquid nitrogen and weighed out in 50 mg aliquots. Smilaside A and smiglaside C were analyzed as described previously (Ding *et al.*, 2017). Negative ionization $[M\text{-}H]^-$ mode scans (0.1-atomic mass unit steps, 2.25 cycles s^{-1}) from *m/z* 100–1000 were acquired. Analyses of smilaside A and smiglaside C peak abundance relied on the native parent $[M\text{-}H]^-$ ion *m/z* 777 and *m/z* 819, and stable average retention times of 12.76 min and 13.94 min, respectively. Both analytes displayed split peaks and for consistency both peaks were integrated and combined for the final analyses.

Data analysis

All *t*-tests were performed with the ttest function implemented in Microsoft EXCEL. ANOVA and Wilcoxon rank sum tests were performed in R. Linear discriminant analysis was performed with SAS software.

Results

Fusarium graminearum-induced root growth inhibition and metabolic reconfiguration are more pronounced in the susceptible maize inbred line B73

Inoculation of maize genotype B73 with *F. graminearum* under controlled growth conditions significantly reduced seedling root growth (Zhou *et al.*, 2018). Using this assay, we screened the 26 parental lines of the maize nested association mapping population (McMullen *et al.*, 2009), as well as inbred lines Mo17 and W22. This showed that B73 was among the most susceptible inbred lines, with root growth being reduced by > 50%. In contrast, Mo17 emerged as one of several potentially

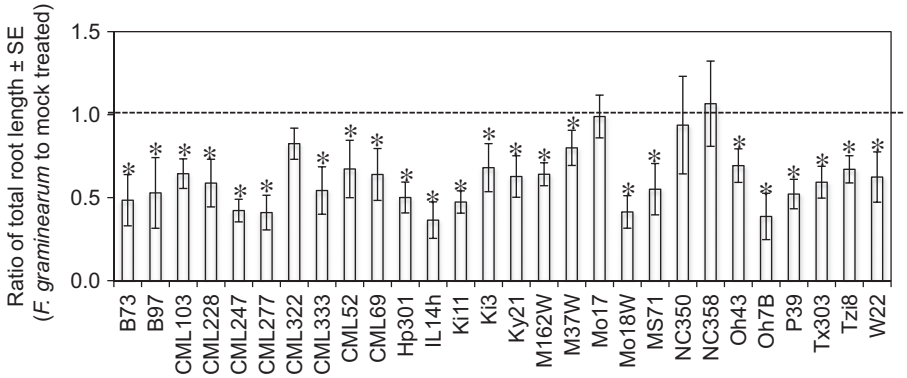

Fig. 1 Natural variation in maize seedling root growth inhibition by *Fusarium graminearum*. The ratio of total root length of *F. graminearum*- to mock-inoculated maize seedlings, measured 6 d post-inoculation, is shown. The dotted line denotes the expected ratio when there is no significant effect of *F. graminearum* infection. At least five mock- and fungus-inoculated individuals were measured for each genotype. *, $P < 0.05$ (Student's *t*-test between treatment groups within the same genotype).

F. graminearum-resistant lines, showing no significant change in root growth after inoculation (Fig. 1, Supporting information Fig. S1). Further research was focused on the B73 vs Mo17 comparison, due to the availability of genetic resources that included RILs and NILs (Lee *et al.*, 2002; Eichten *et al.*, 2011). The higher fungal resistance of Mo17 was confirmed by lower expression of *FgTUB*, a *F. graminearum*-specific tubulin gene, lower concentrations of deoxynivalenol, a mycotoxin produced by *F. graminearum*, and fewer visible necrotic symptoms in the roots (Fig. 2a–c).

We hypothesized that the contrasting *F. graminearum* resistance levels in B73 and Mo17 seedling roots could be attributed to differences in their constitutive and/or inducible biochemical defenses. Therefore, we performed nontargeted comparative metabolomic analyses of B73 and Mo17 seedling roots, with and without *F. graminearum* inoculation. Consistent with the difference in *F. graminearum*-induced root growth reduction between these two inbred lines, we observed that > 300 mass features were significantly altered by *F. graminearum* infection of B73, but only 20 were altered in Mo17 in this experiment (Fig. 2d).

Acetylated diferuloylsucroses contribute to *F. graminearum* resistance

In order to identify specific metabolites that could contribute to the contrasting *F. graminearum* resistance levels in B73 and Mo17, a separate nontargeted metabolomic experiment was performed to compare the constitutive metabolomes of B73 and Mo17 seedling roots, as well as mock- and *F. graminearum*-inoculated B73 seedling roots. This identified 40 mass features that were both significantly affected by *F. graminearum* in the susceptible B73 seedling roots and constitutively different between B73 and Mo17 seedling roots (Tables S1–S3). Among these 40 mass features, several represented specialized metabolites with known antifungal activity, including benzoxazinoids and phenylpropanoids (Bollina *et al.*, 2010; Ponts *et al.*, 2011; Kazan *et al.*, 2012).

Two mass features with *m/z* 819.2321 and 777.2221 under negative ESI mode, eluting at 6.11 and 5.61 min, respectively, were significantly induced by *F. graminearum* infection of both B73 and Mo17 seedling roots. In all samples, the *m/z* 819 metabolite was much more abundant than the *m/z* 777 metabolite (Fig. 3a,b). B73 contained significantly more of the *m/z* 819 metabolite than Mo17, both constitutively and after *F. graminearum* induction (Fig. 3a). By contrast, the *m/z* 777 metabolite was more abundant in Mo17 under both conditions (Fig. 3b).

The *m/z* 819 metabolite was identified as 3,6-diferuloyl-2′,3′,6′-triacetylsucrose (Fig. 3d), based on its phenylpropanoid-like UV absorbance profiles (Fig. S2), MS/MS (Fig. S2), and NMR spectroscopy (HSQC, HMBC and dqfCOSY spectra; Table S4). Based on the MS/MS data and difference in exact mass, the *m/z* 777 metabolite was predicted to have one fewer acetyl group. This was confirmed by 1D proton NMR, which showed that the C2′ acetyl group was absent, and the compound was 3,6 diferuloyl-3′,6′-diacetylsucrose (Fig. 3e; Table S4). These two metabolites were previously identified as smilaside A (3,6 diferuloyl-3′,6′-diacetylsucrose) in *Smilax china* (Kuo *et al.*, 2005) and smiglaside C (3,6-diferuloyl-2′,3′,6′-triacetylsucrose) in *Smilax glabra* (Chen *et al.*, 2000).

In addition to smilaside A and smiglaside C, other maize compounds co-eluted with a UV-absorbance peak at 328 nm, characteristic of a phenylpropanoid moiety. These included likely structural isomers of smilaside A and smiglaside C, with identical *m/z* ratio and different retention times, as well as possible monoacetylated (*m/z* = 735.21) and tetraacetylated (*m/z* = 861.24) diferuloylsucroses (Fig. S3). However, the structures of these other maize metabolites were not confirmed, and their functions were not investigated in this study. Notably, nonacetylated diferuloylsucrose (expected *m/z* = 693.21) was not detected.

The structural resemblance of smilaside A and smiglaside C suggested that they could be the substrate and product of an acetylation/deacetylation reaction. This reaction was probably actively regulated upon fungal infection, with *F. graminearum* infection inducing a significant increase in the smilaside A : smiglaside C ratio only in the resistant Mo17 seedlings, but not in the susceptible B73 ones (Fig. 3c). This induced response

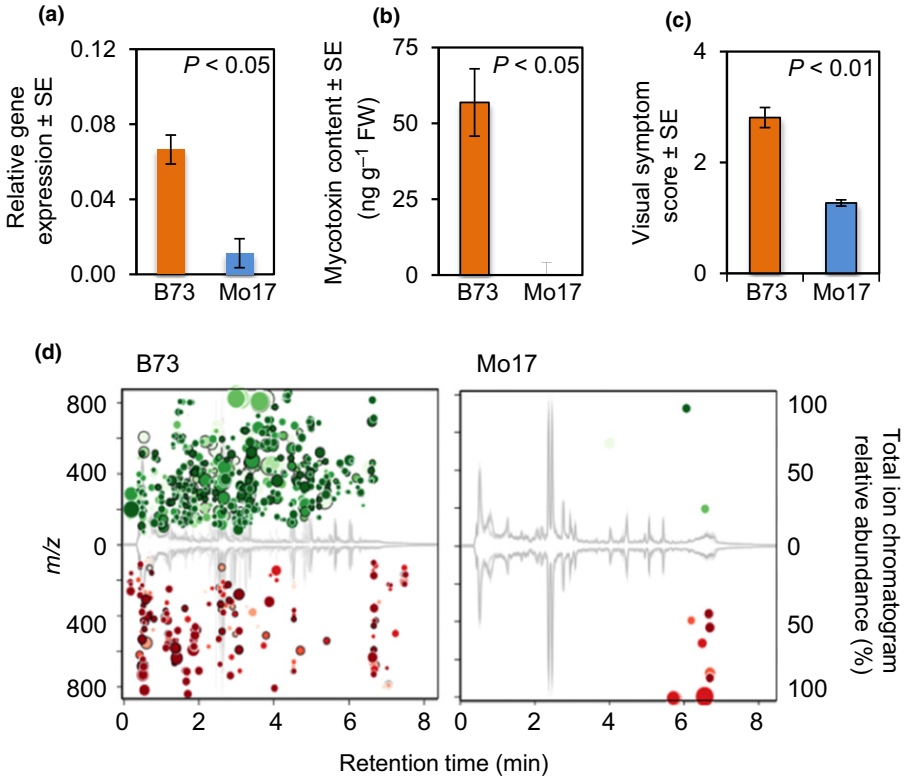

Fig. 2 Mo17 is more resistant to *Fusarium graminearum* than B73. Compared to B73, Mo17 seedling roots inoculated with *F. graminearum* demonstrate: (a) lower expression of an *F. graminearum*-specific α-tubulin gene, mean ± SE of $n = 5$; (b) lower content of deoxynivalenol at 6 d post inoculation, mean ± SE of $n = 5$; and (c) reduced symptoms on a 0–4 scale (0 = no symptoms to 4 = seedling death, mean ± SE of $n = 10$. *, $P < 0.05$ (a, b, two-tailed unpaired Student's *t*-tests; c, paired *t*-test)). (d) Nontargeted metabolomics of *F. graminearum*-inoculated B73 and Mo17 seedling roots under negative electron spray ionization mode. For either genetic background, each mass feature that was significantly different between treatments (control vs infected, $n = 5$; $P < 0.05$; fold-change > 1.5) was plotted as a bubble on the total ion current chromatogram, with its size proportional to the fold-change, and darker color representing a more significant change. Mass features induced by *F. graminearum* are shown in the upper half of each plot and *F. graminearum*-suppressed mass features are shown in the lower half. *m/z*, mass-to-charge ratio.

suggested that smiglaside C and/or smilaside A could play a role in maize biochemical defense against *F. graminearum*. *In vitro* fungal growth inhibition assays were conducted in liquid suspension culture using smiglaside C and smilaside A concentrations similar to those found in maize seedlings (Fig. S4). Although present a lower concentration, smilaside A showed a more significant inhibition of *F. graminearum* growth *in vitro* than smiglaside C (Fig. 3f). This was consistent with our earlier observation that the *F. graminearum*-resistant Mo17 seedlings had a higher constitutive smilaside A content, and further accumulated this compound upon fungus attack compared to the susceptible B73 seedlings (Fig. 3a–c).

Genetic mapping of smiglaside C and smilaside A abundance identifies *ETHYLENE INSENSITIVE 2* as a candidate regulator

The constitutive difference in smilaside A and smiglaside C abundance between B73 and Mo17 seedling roots allowed us to investigate the genetic control of this natural variation (Table S5). Composite interval mapping with seedling roots of 83 RILs from the intermated B73 × Mo17 (IBM) population (Lee *et al.*, 2002; Wang *et al.*, 2012) showed that the most significant QTL for both metabolites was located at the same position on chromosome 3 (Fig. 4a). Interestingly, the two QTL had opposite effects, with the B73 allele promoting constitutive smiglaside C abundance and reducing smilaside A abundance (Fig. 4b,c). Because smilaside A and smiglaside C were likely the substrate-product pair of an acetylation/deacetylation reaction, we hypothesized that the mapped QTL could regulate the efficiency of this reaction. We identified the same locus when mapping the smilaside A : smiglaside C ratio as a quantitative trait, with the B73 allele reducing the smilaside A : smiglaside C ratio (Fig. S5).

In order to further confirm the role of this QTL in regulating the relative abundance of smiglaside C and smilaside A, we quantified the metabolites in B73-Mo17 NILs with reciprocal introgressions at this locus (Eichten *et al.*, 2011). Consistent with the RILs results, the smilaside A : smiglaside C ratio showed clear co-segregation with the genetic markers at the chromosome 3 QTL, with the NILs carrying the B73 allele having a lower ratio, irrespective of their genetic background (Fig. 4d). A significant difference between NILs carrying either allele also was observed for smilaside A but not smiglaside C ($P = 0.075$; Fig. S6). Furthermore, due to additional recombination breakpoints and denser genetic marker data available for the NILs, we narrowed down the QTL region to *c.* 630 kb pairs (kbps), containing 22

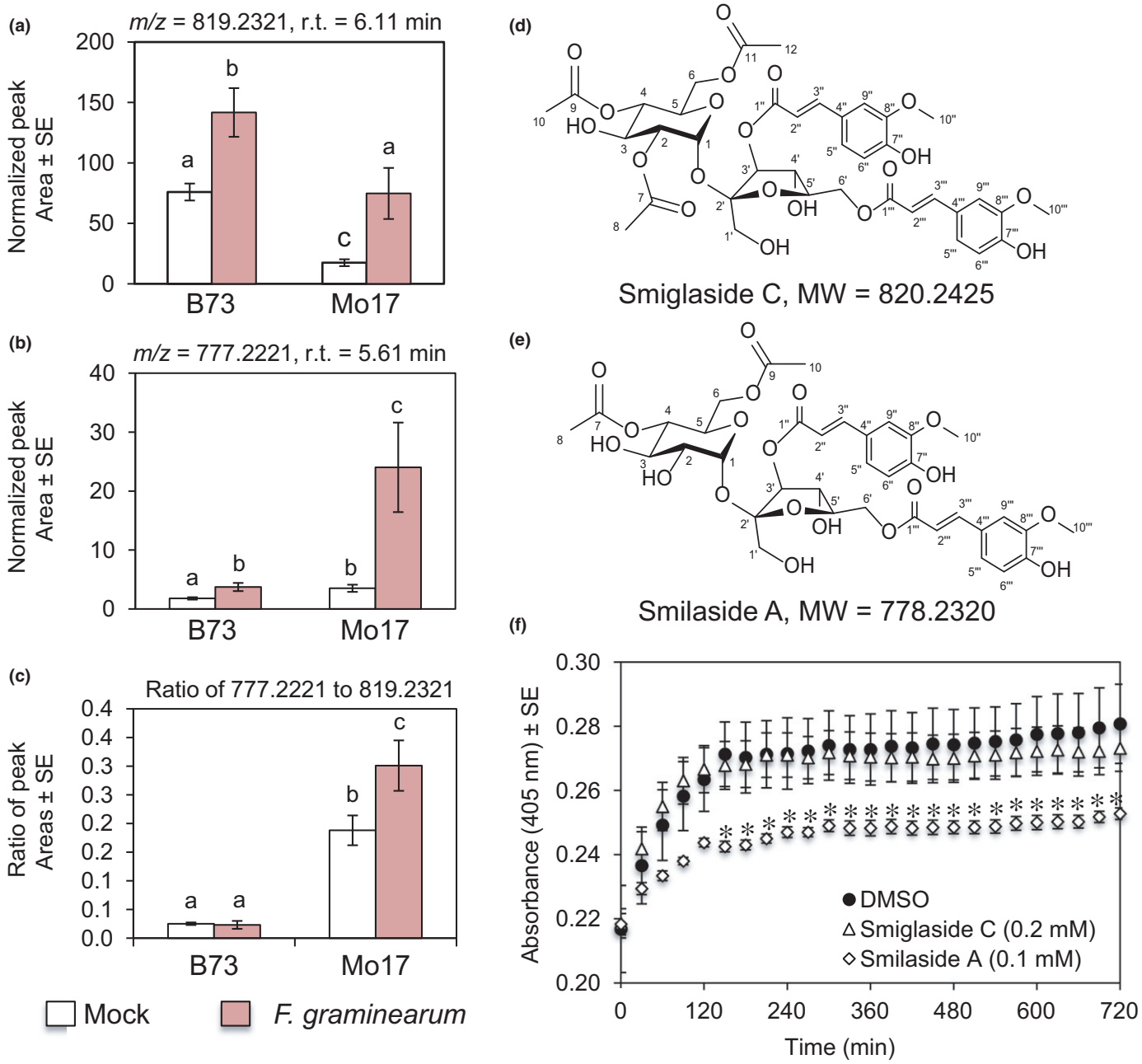

Fig. 3 Antifungal metabolites smiglaside C and smilaside A are differentially induced by *Fusarium graminearum* in B73 and Mo17. Abundance of metabolites with (a) *m/z* 819 and (b) *m/z* 777 was measured in negative electron spray ionization mode (*m/z*, mass-to-charge ratio). (c) Ratio of the peak areas of the two metabolites. Mean ± SE of $n = 4$. Different letters indicate significant differences, $P < 0.05$ (ANOVA followed by Tukey's HSD test). Structures of (d) smiglaside C and (e) smilaside A were determined by LC-MS/MS and NMR. (f) Growth of an *F. graminearum* spore/hyphae suspension incubated with smilaside A, smiglaside C or a dimethylsulfoxide (DMSO) solvent-only control. Fungal growth was monitored by absorbance at 405 nm. Mean ± SE of $n = 4$; *, $P < 0.05$ (Student's *t*-test relative to the DMSO control at the same time point). MW, molecular weight.

predicted gene models in the maize inbred line B73 Refgen v3 genome (Schnable *et al.*, 2009).

Natural variation in metabolic traits is often caused by *cis* polymorphisms in metabolic enzyme-encoding genes (Meihls *et al.*, 2013; Yan *et al.*, 2015; Handrick *et al.*, 2016). However, we found no predicted acetyltransferase gene within our QTL interval. Moreover, by plotting the distribution of smiglaside C and smilaside A across the IBM RILs, we found an overall positive correlation between these two metabolites (Fig. 5a), which contradicted the prediction of polymorphism in a hypothetical acetyltransferase that would catalyze the interconversion of these two metabolites. Closer investigation of the smiglaside C–smilaside A distribution plot revealed that the 83 RILs can be divided by linear discriminant analysis into a B73-like group with lower smilaside A : smiglaside C ratios, and a Mo17-like group with higher ratios (Fig. 5a). We hypothesized

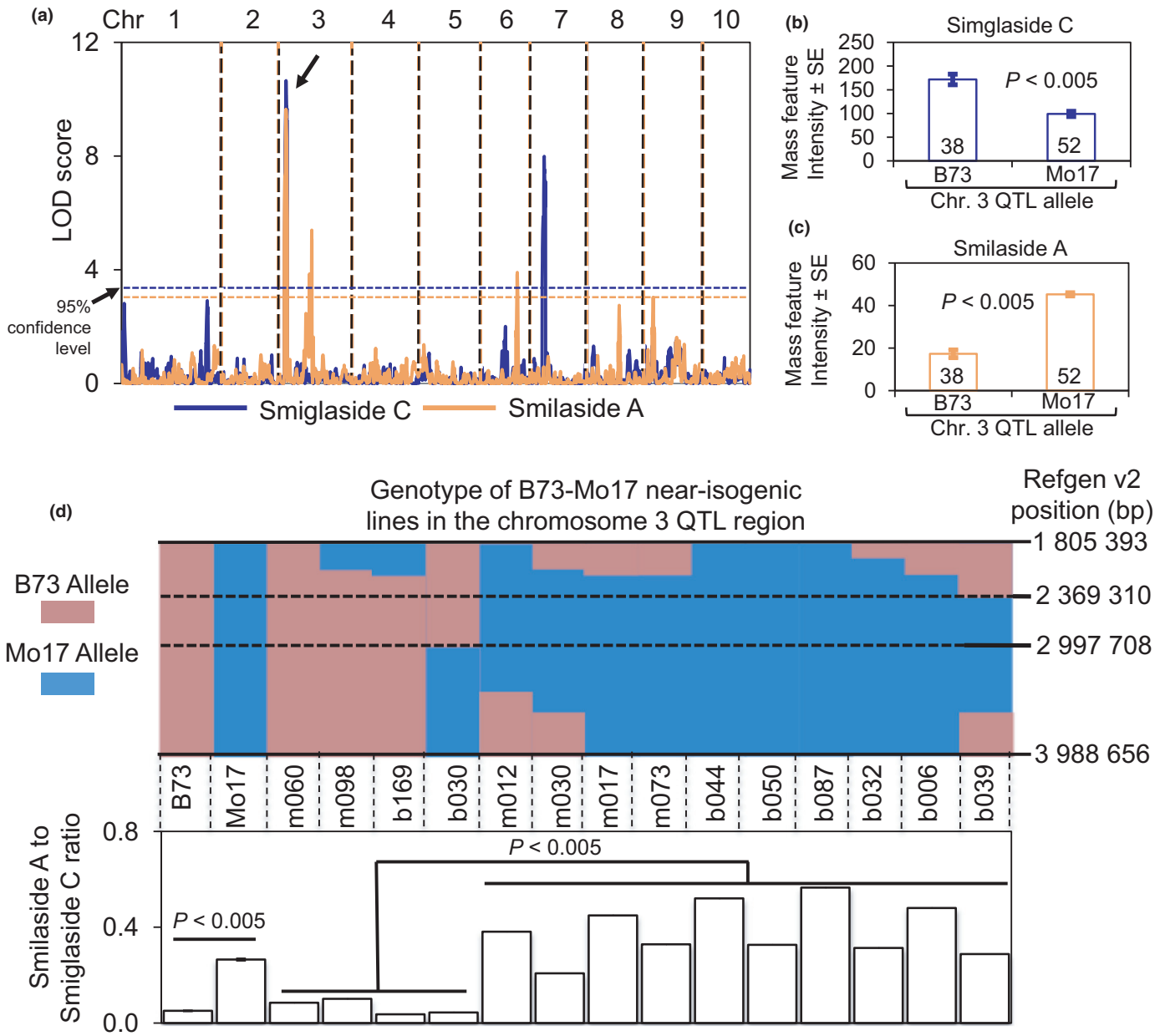

Fig. 4 Smiglaside C and smilaside A share a quantitative trait locus (QTL) on maize chromosome 3 with opposite effects. (a) Composite interval mapping of smiglaside C (blue) and smilaside A (orange) in the seedling roots of B73 × Mo17 recombinant inbred lines (RILs) identified a significant QTL for both traits on chromosome 3 (indicated by an arrow). RILs with the B73 QTL allele on chromosome 3 have (b) more smiglaside C and (c) less smilaside A than those with the Mo17 allele. Numbers in bars are sample sizes. *P*-values were determined with two-tailed Student's *t*-tests. (d) The smilaside A : smiglaside C ratio was calculated for B73, Mo17 and near-isogenic lines (NILs). The genetic background of the NILs is indicated by the initial letter of the line name, for example, m060 has a Mo17 genetic background and b169 has a B73 genetic background. The smilaside A : smiglaside C ratio is higher in Mo17 than in B73 (mean ± SE of $n = 3$, Student's *t*-test). NILs carrying the Mo17 allele at the Chromosome 3 QTL have a higher smilaside A : smiglaside C ratio than those with the B73 allele (Students *t*-test), irrespective of the overall genetic background. LOD, log of odds.

that this phenotypic difference could be attributed to transcriptional regulation, which would differ between the IBM RILs belonging to either phenotypic group. We therefore performed whole transcriptome profiling on the seedling root samples that were used for metabolite quantification. This analysis showed that the genes with the most significant differential expression between the two phenotypic groups were located in the identified QTL region on chromosome 3 (Fig. 5b,c; Table S6). Specifically, the gene showing the most significantly different expression was a positive regulator of ethylene signaling in maize, *ZmEIN2* (*ETHYLENE INSENSITIVE* 2; GRMZM2G 068217), which was expressed at a significantly higher level in the seedling roots of RILs with B73-like abundance of smiglaside C and smilaside A (Fig. 5d). This led to the hypothesis that *ZmEIN2* is a negative regulator of smilaside A : smiglaside C ratio.

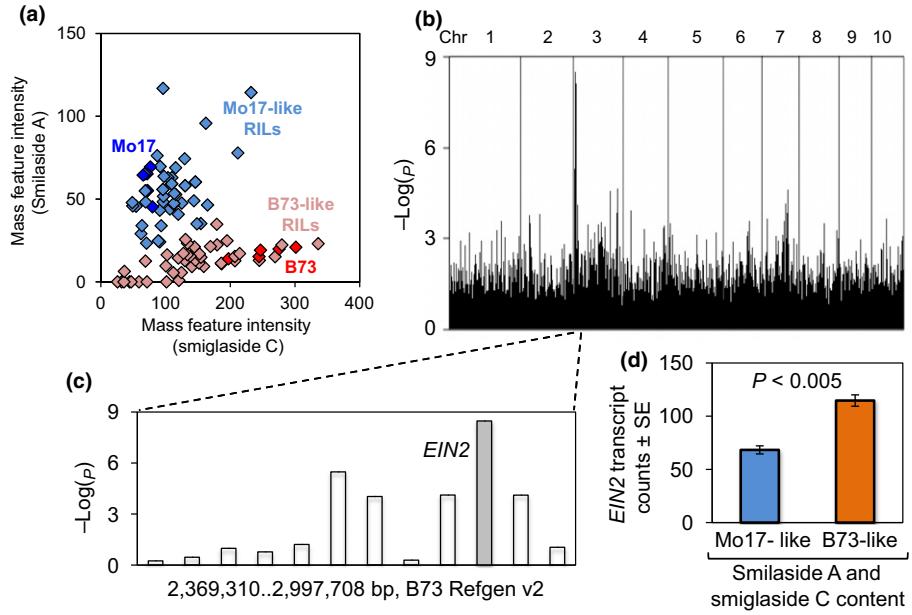

Fig. 5 *ETHYLENE INSENSITIVE 2* (*EIN2*) is differentially expressed in maize B73 × Mo17 recombinant inbred lines (RILs) with contrasting smilaside A : smiglaside C ratios. (a) B73 × Mo17 RILs can be divided into two groups based on their constitutive smilaside A and smiglaside C content. One replicate each of 83 B73 × Mo17 RILs and five replicates of the B73 and Mo17 parental lines were plotted based on the constitutive content of smilaside A and smiglaside C in their seedling roots. The parental lines are indicated with dark blue (Mo17) and dark red (B73). The RILs were determined to be Mo17-like (light blue) or B73-like (light red) in their smilaside A and smiglaside C content using the linear discriminant analysis. The level of significance in differential expression between Mo17- and B73-like inbred lines, measured by $-\log(P)$ from Student's *t*-tests, is plotted for each root-expressed transcript in the chromosomal order across the whole genome (b) and within the quantitative trait locus region on chromosome 3 (c). (d) Expression of *EIN2* is significantly higher in the seedling roots of RILs with a B73-like smilaside A and smiglaside C content than in ones with a Mo17-like content. Mean ± SE, *P*-value is from a two-tailed Student's *t*-test. chr, chromosome.

Acetylated feruloylsucrose accumulation and resistance against *F. graminearum* are regulated by ethylene and the *ZmEIN2*-containing QTL

No *ZmEIN2* mutation is available in public maize transposon insertion collections. Instead, we manipulated ethylene response *in vivo* with a gaseous competitive inhibitor, 1-methylcyclopropene (1-MCP), and a biochemical precursor of ethylene production in plant, 1-aminocyclopropane-1-carboxylic acid (1-ACC) in B73 seedlings. The effects of these treatments were confirmed by contrasting seedling growth rate in these groups (Fig. S7). Consistent with the genetic mapping results, 1-MCP treatment led to hyper-accumulation of smilaside A and Smiglaside C, and an elevated smilaside A : smiglaside C ratio (Fig. 6a–c). Both smilaside A and smiglaside C were induced by 1-ACC treatment, but their ratio was not significantly affected (Fig. 6a–c). Because there is no known functionally redundant gene for *ZmEIN2* (Yang *et al.*, 2015; Gallie & Young, 2004), we hypothesized that the ethylene-induced change in the smilaside A : smiglaside ratio was mediated by the *ZmEIN2*-containing QTL identified above. In support of this hypothesis, 1-ACC treatment significantly increased the smilaside A : smiglaside C ratio in both Mo17 and NILs carrying the Mo17 *ZmEIN2* allele, but not in B73 or NILs carrying the B73 allele of this gene (Fig. 7a). The difference in constitutive *ZmEIN2* expression in seedling roots between the two parental lines was not significant in this experiment, perhaps due to the small number of replicates (three per line). However, NILs carrying the B73 allele at this QTL showed significantly higher *ZmEIN2* expression than those carrying the Mo17 allele (Fig. 7b).

In order to further investigate how smilaside A and smiglaside C were regulated by ethylene production, we measured their abundance in the seedling roots of the *Zmacs2-1 Zmacs6* ethylene biosynthetic mutant, which has *Mutator* transposon insertions in two 1-ACC synthase genes in the B73 genetic background (Young *et al.*, 2004). Consistent with prior measurement of lower leaf ethylene content, this double mutant had a lower root ethylene concentration than wild-type (WT) (Fig. S8). Metabolite abundance was measured with and without exogenous 1-ACC, which is downstream of the two mutated *ZmACS* genes in the ethylene biosynthetic pathway. Constitutively, there were significantly lower amounts of both smilaside A and smiglaside C in the roots of *Zmacs2-1 Zmacs6* compared to WT B73. After 1-ACC treatment, both metabolites were increased in WT B73, and were restored to WT levels in *Zmacs2-1 Zmacs6* (Fig. 8a,b). In *Zmacs2-1 Zmacs6*, the smilaside A : smiglaside C ratio was significantly lower than in WT B73. Consistent with results from the previous experiment, 1-ACC treatment did not affect this ratio in either genetic background (Fig. 8c).

In order to investigate how ethylene and the acetylated feruloylsucroses can affect maize seedling defense against *F. graminearum*, we compared *F. graminearum*-inoculated maize seedling roots treated with 1-ACC, 1-MCP or water control. We observed extensive fungal hyphae of the GFP-transformed

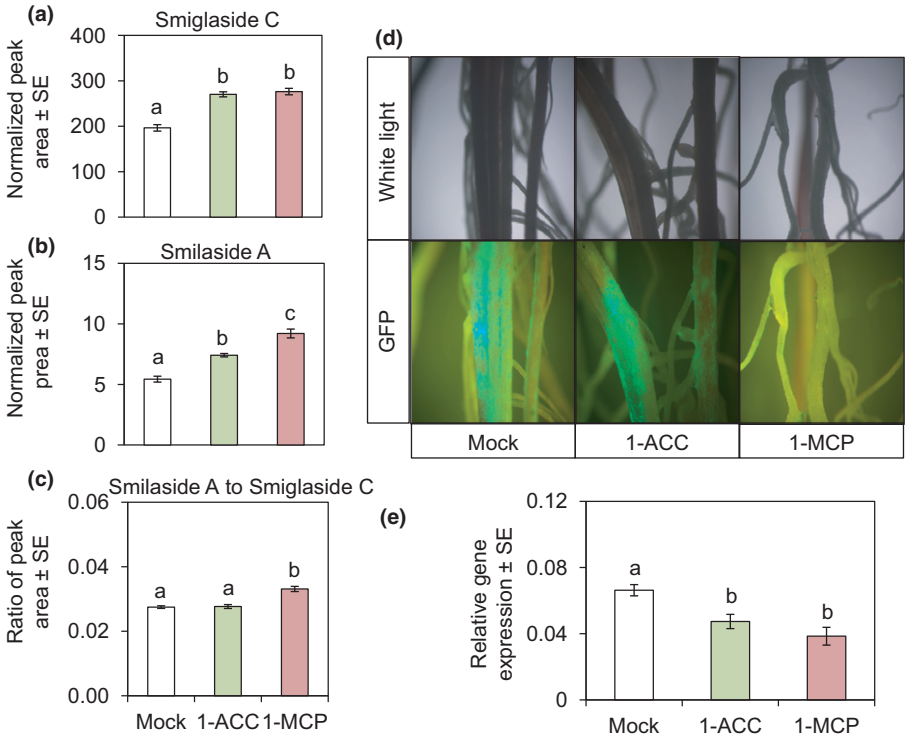

Fig. 6 Exogenous 1-aminocyclopropane-1-carboxylate (1-ACC) and 1-methylcyclopropene (1-MCP) treatment promote acetylated feruloylsucrose accumulation and *Fusarium graminearum* resistance in maize seedlings. B73 maize seedling roots inoculated with *F. graminearum* were treated with 1-ACC, 1-MCP or water as a control. The abundance of (a) smiglaside C, (b) smilaside A and (c) the ratio of the two metabolites was calculated from peak area under negative electron spray ionization mode. Mean ± SE of $n = 5$, different letters indicate significant difference, $P < 0.05$ (ANOVA followed by Tukey's HSD test). (d) B73 maize seedling roots inoculated with green fluorescence protein (GFP)-transformed *F. graminearum* and treated with 1-ACC, 1-MCP or mock treatment for 10 d were examined with white light and fluorescence microscopy. More GFP marker expression from *F. graminearum* was observed on root surface of mock- and 1-ACC treated seedling roots than on 1-MCP-treated roots. (e) Fungal growth was quantified by quantitative reverse transcription polymerase chain reaction (qRT-PCR) using *F. graminearum*-specific primers, relative to expression measurement of a maize housekeeping gene. Mean ± SE of $n = 8$, different letters indicate significant differences, $P < 0.05$ (ANOVA followed by Tukey's HSD test).

F. graminearum on the root surface of both mock-treated seedlings, lesser amounts on 1-ACC-treated roots and almost complete absence from 1-MCP-treated roots (Fig. 6d). In support of the microscopic observations, *FgTUB* expression was significantly lower in 1-ACC- and 1-MCP-treated seedling roots (Fig. 6e). Neither 1-ACC nor 1-MCP affected growth of *F. graminearum* on agar plates (Fig. S9), suggesting no direct toxic effect. Across B73 × Mo17 NILs with reciprocal introgressions at the *ZmEIN2*-containing QTL, those carrying the Mo17 alleles were significantly more resistant to *F. graminearum* than those carrying the B73 allele, as measured by visual symptom scoring (Fig. 7c,d). The overall genetic background of the lines (m = Mo17 and b = B73) did not have a significant effect on symptom development (Fig. 7e). Comparing infected seedling roots of *Zmacs2-1 Zmacs6* and WT B73, we found significantly higher *F. graminearum* growth on the mutant line (as measured by ergosterol accumulation; Fig. 8d).

Maize diferuloylsucroses are induced by multiple fungal pathogens

A mass feature likely representing smiglaside C was identified as a maize acyl sugar that was induced after infection with *Colletotrichum graminicola* (anthracnose leaf blight), although without structural confirmation (Balmer *et al.*, 2013). To determine whether induced production of smilaside A and smiglaside C is a more general maize response to fungal infection, we inoculated seedlings with four additional fungal pathogens, *A. flavus*, *R. microspores*, *F. verticilloides* and *C. heterostrophus*. Whereas smilaside A was only induced by *F. verticilloides* and *C. heterostrophus*, all four pathogens significantly induced the accumulation of smiglaside C (Fig. 9). As in the case of *F. graminearum* infection (Fig. 3a–c), smiglaside C was induced to a greater extent than smilaside A. Therefore, induced accumulation of smiglaside C may be a general response of maize to infection by fungal pathogens.

Discussion

Acetylated feruloylsucroses were first identified in the rhizomes of *Smilax china* and *S. glabra*, which are used in traditional Chinese medicine (Chen *et al.*, 2000; Kuo *et al.*, 2005). Similar phenylpropanoid sucrose esters, with different numbers and types of phenylpropanoid groups attached, were later found in various Liliaceae and Polygonaceae species. Crude plant extracts containing these compounds, and in some cases purified compounds,

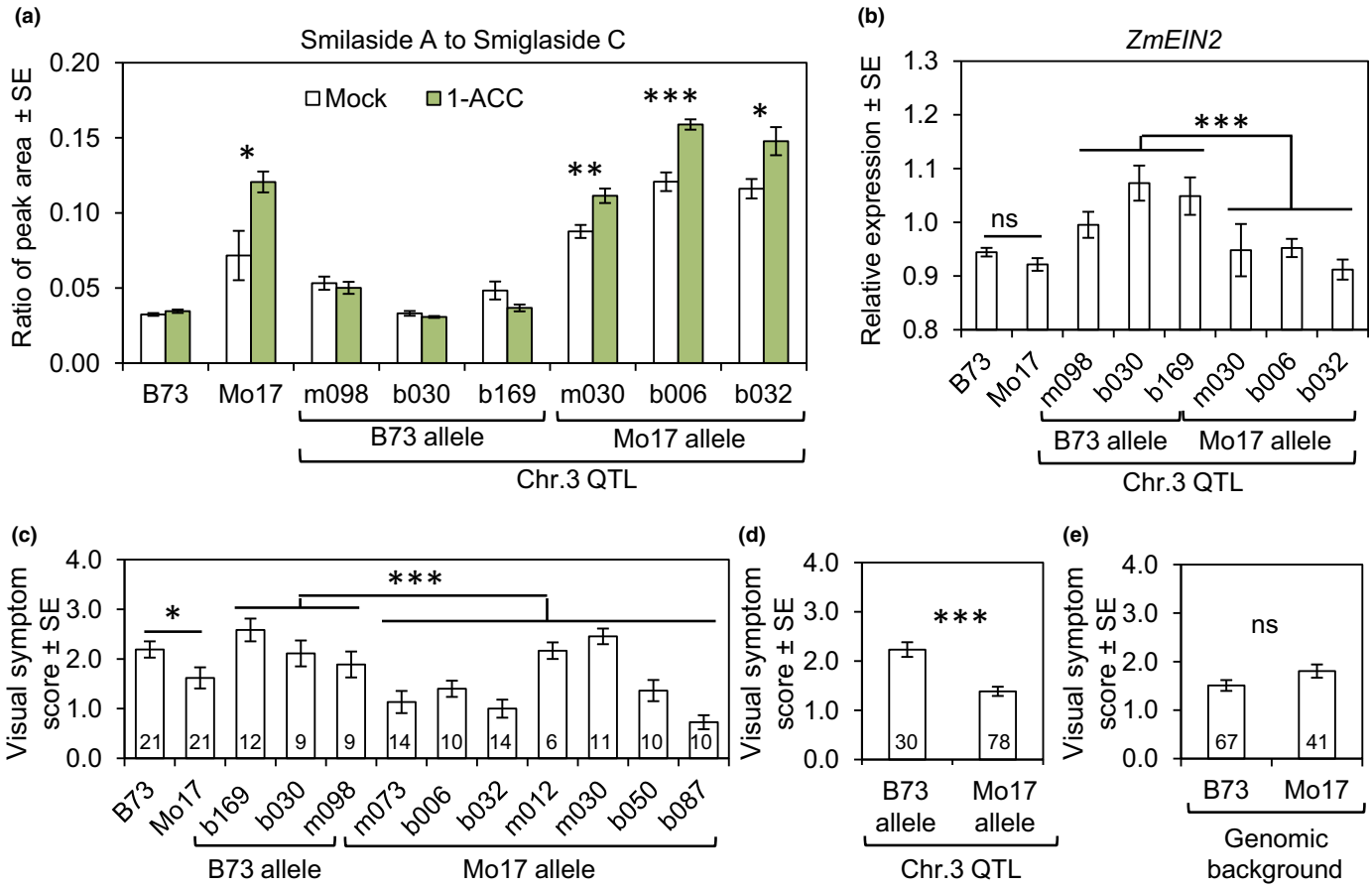

Fig. 7 *ZmEIN2* expression, 1-aminocyclopropane-1-carboxylate (1-ACC)-induced shift in smilaside A : smiglaside C ratio, and *Fusarium graminearum* resistance co-segregate across B73 × Mo17 near isogenic lines (NILs) segregating at the quantitative trait locus (QTL) containing *ZmEIN2*. Ten-day-old seedlings of B73, Mo17 and NILs segregating at the *ZmEIN2* locus were treated with 1-ACC or water control (mock) for three consecutive days. (a) The smilaside A : smiglaside C ratio was calculated from the peak areas under negative electron spray ionization mode. Mean ± SE of $n = 5$. (b) *ZmEIN2* expression in mock-treated NIL and parental seedling roots was measured by quantitative reverse transcription polymerase chain reaction (qRT-PCR), normalized by maize actin expression in each replicate. Mean ± SE of $n > 3$. (c) Ten-day-old seedlings of B73, Mo17 and NILs segregating at the *ZmEIN2* locus were inoculated with *F. graminearum* spores, and visual symptoms were scored on the same 0–4 scale. Mean ± SE of visual symptom scores. (d) Average of NILs carrying either the B73 or the Mo17 allele at the QTL containing *ZmEIN2*. (e) Average of NILs of having either the B73 or the Mo17 genomic background. The number of replicates for each genotype is indicated at the bottom of the respective column. For all panels (Student's *t*-tests): ns, not significant; *, $P < 0.05$; **, $P < 0.01$; ***, $P < 0.005$.

have shown anticancer and antioxidant activities *in vitro* (Zhu *et al.*, 2006; Ono *et al.*, 2007; Yan *et al.*, 2008; Zhang *et al.*, 2008; Kim *et al.*, 2010). Building on these promising *in vitro* bioactivities, organic synthesis routes to produce natural phenylpropanoid sucrose esters and structural analogs have been developed (Panda *et al.*, 2012a,b). More recently, this class of metabolites has been found in rice (Chen *et al.*, 2014; Cho *et al.*, 2015). In the current study, two acetylated feruloylsucroses, smilaside A and smiglaside C, were shown to be induced by fungal infection in maize (Figs 3a–c, 9).

In vitro assays with purified compounds showed that the diacetylated smilaside A caused greater fungal growth inhibition than the triacetylated smiglaside C (Fig. 3f). This was perhaps surprising, because phenylpropanoid sucrose esters with higher degrees of acetylation had generally shown stronger *in vitro* bioactivities, although these two specific compounds had not been compared previously (Panda *et al.*, 2012b; Cho *et al.*, 2015). Our observations suggest a more complex relationship between the degrees of acetylation and bioactivity, which may also be distinct between different structural isomers. Other than the putative tetra-acetylated diferuloylsucrose, all acetylated diferuloylsucroses detected in our LC-MS analyses showed signs of multiple structural isomers, although there was usually a predominant one (Fig. S2).

Our discovery of smilaside A and smiglaside C in maize will facilitate the *in planta* investigation of phenylpropanoid sucrose ester function and metabolism. Quantification of smilaside A and smiglaside C across Intermated B73 × Mo17 (IBM) recombinant (RILs) and near-isogenic inbred lines (NILs) identified a 630 kbp locus on maize chromosome 3 as a regulator of these two metabolites (Figs 4, S4, S5). Across both populations, the expression of *ZmEIN2,* located within this quantitative trait locus (QTL), negatively correlated with the smilaside A : smiglaside C ratio (Figs 5, 7a,b). This led to the hypothesis that ethylene signaling promoted preferential accumulation of smiglaside C over smilaside A, because *EIN2* was required for

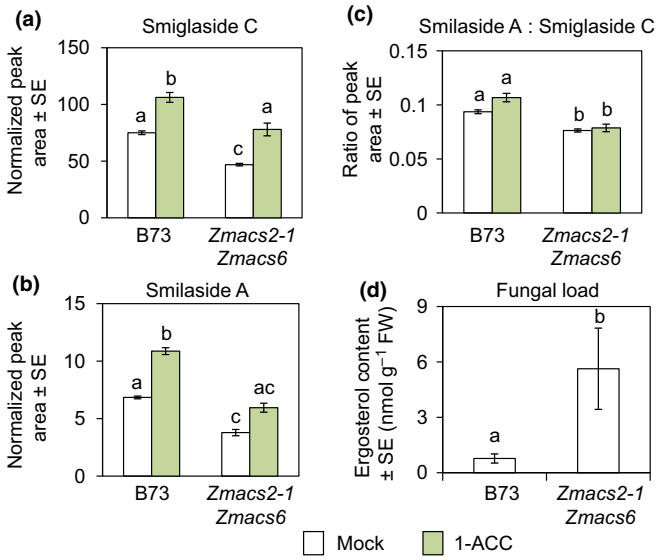

Fig. 8 Ethylene biosynthesis is required for acetylated feruloylsucrose accumulation and resistance against *Fusarium graminearum*. The abundance of (a) smiglaside C and (b) smilaside A was estimated by peak area at their respective mass-to-charge ratio (*m*/*z*) under negative electron spray ionization mode in a maize aminocyclopropane-1-carboxylate synthase double mutant (*Zmacs2-1 Zmacs6*) and its wild-type progenitor B73. (c) The ratio of smilaside A to smiglaside C peak areas. Mean ± SE, different letters indicate significant differences, $P < 0.05$ (two-way ANOVA followed by Tukey's HSD test). (d) Fungal load was estimated by ergosterol content, normalized by root tissue FW. Mean ± SE, different letters indicate significant differences, $P < 0.05$ (one-way ANOVA).

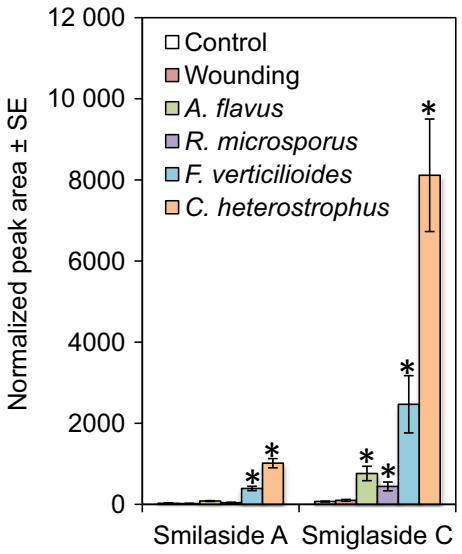

Fig. 9 Smilaside A and smiglaside C are induced by fungal pathogen infection. Smilaside A and smiglaside C content was measured in 35-d-old Mo17 stem tissues 4 d after physical wounding or inoculation with *Aspergillus flavus*, *Rhizopus microspores*, *Fusarium verticilloides* or *Cochliobolus heterostrophus*. Mean ± SE of $n = 4$. *, $P < 0.05$ (relative to the uninfected control, pairwise Wilcoxon rank sum tests with Benjamini and Hochberg correction for multiple comparisons).

functional ethylene signaling, a pathway that is well conserved across representative monocot and eudicot species (Yang *et al.*, 2015). In support of this hypothesis, exogenous treatment with 1-methylcyclopropene (1-MCP), a competitive inhibitor of ethylene signaling, elevated the smilaside A : smiglaside C ratio and the absolute abundance of both metabolites in B73 seedling roots, whereas exogenous 1-aminocyclopropane-1-carboxylic acid (1-ACC) induced accumulation of both metabolites without affecting their relative abundance (Fig. 6a–c). Interestingly, the smilaside A : smiglaside C ratio can be induced by 1-ACC in Mo17 and NILs carrying the Mo17 allele at the *ZmEIN2*-containing QTL, but not in NILs with the B73 allele (Fig. 7a). This suggests that the B73 and Mo17 alleles of this QTL, and presumably *ZmEIN2*, mediate the differential metabolic responses to 1-ACC treatment. Furthermore, analyses of a maize ethylene biosynthetic mutant, *Zmacs2-1 Zmacs6* demonstrated that ethylene production was sufficient and necessary for the accumulation of both smilaside A and smiglaside C. Whereas exogenous 1-ACC supplementation had no effect on the ratio of the two metabolites in either wild-type or mutant seedlings, genetic perturbation of ethylene biosynthesis led to a reduced smilaside A : smiglaside C ratio, in addition to lower absolute abundance of both metabolites (Fig. 8). Together, these results indicate that baseline ethylene production in maize is required for the accumulation of acetylated feruloylsucroses in general, whereas the relative abundance of smilaside A and smiglaside C specifically is negatively regulated by ethylene responses.

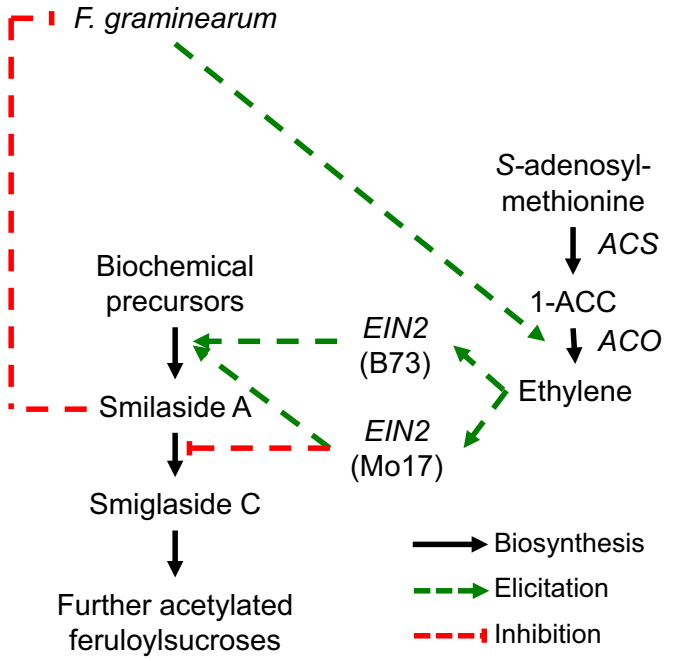

Fig. 10 Ethylene regulation of acetylated feruloylsucrose metabolism in maize seedling roots upon *Fusarium graminearum* infection. Fungal infection induces ethylene production, which leads to differential effects on acetylated feruloylsucrose metabolism, depending on allelic difference in *ZmEIN2*, and preferential accumulation of either smilaside A in Mo17 or smiglaside C in B73. This could contribute to the natural variation in *F. graminearum* resistance in the B73 and Mo17 maize inbred lines. 1-ACC, 1-aminocyclopropane-1-carboxylate; ACS, 1-aminocyclopropane-1-carboxylate synthase; ACO, 1-aminocyclopropane-1-carboxylate oxidase; EIN2, ethylene insensitive 2.

Fusarium graminearum infection was known to induce ethylene biosynthetic and responsive genes in both maize seedling roots (Ye *et al.*, 2013) and *Brachypodium distachyon* spikes (Pasquet *et al.*, 2014). Different comparative transcriptomic studies in wheat had reached opposite conclusions regarding the role of ethylene signaling in responses to *F. graminearum* infection (Li & Yen, 2008; Ding *et al.*, 2011; Xiao *et al.*, 2013). In both wheat and barley leaves, *F. graminearum* resistance could be manipulated by interfering with ethylene signaling (Chen *et al.*, 2009). In this study, we observed that maize seedlings with lower *ZmEIN2* expression or artificially treated with 1-MCP were more resistant to *F. graminearum* and preferentially accumulate the more bioactive smilaside A (Figs 3 and 6). However, exogenous ethylene supplementation in the form of 1-ACC also enhanced maize seedling root resistance against *F. graminearum*, which is different from what was reported previously in wheat and barley leaves treated with ethylene gas (Fig. 6; Chen *et al.*, 2009). Furthermore, genetic knockdown of ethylene biosynthesis led to a lower smilaside A : smiglaside C ratio, and rendered the seedlings more susceptible to *F. graminearum* (Fig. 7). This inconsistency could arise from differences in plant species, tissue type, developmental stage or the treatment regime. Together, these results indicate that although ethylene production is required for maize biochemical defense, ethylene sensitivity negatively regulates the efficiency of this biochemical defense. This balance in the abundance of different specialized metabolites could lead to contrasting degrees of fungal resistance (Fig. 10).

Because acetylated feruloylsucroses can be induced by several fungal pathogens in maize, it would be interesting to assess their crop protection value *in vivo* under more relevant field conditions. Simple phenylpropanoids could contribute to disease resistance not only through their direct antimicrobial activities, but also by playing a role in physical fortification of plant cell walls (Nicholson & Hammerschmidt, 1992). The importance of cell walls as a physical barrier against *F. graminearum* and other fungal pathogens was highlighted by the prevalence of genes that likely encode cell-wall-degrading enzymes in the genomes of fungal phytopathogens (Cuomo *et al.*, 2007; Kubicek *et al.*, 2014). Should acetylated feruloylsucroses also contribute to the physical strength of plant cell walls, such effects would not be evident in *in vitro* assays.

Assessment of acetylated feruloylsucrose function *in planta* could be achieved through genetic manipulation of their biosynthetic genes. Although our study has not revealed any enzyme-encoding genes that are involved directly in the biosynthesis of the metabolites of interest, the chemical structures of smilaside A and smiglaside C shed light on their possible biosynthetic pathway. Specifically, we hypothesize that distinct but related hydroxycinnamoyl transferases are responsible for the esterification of feruloyl-CoA and the free hydroxyl groups on the sucrose molecule. The B73 Refgen v3 genome contains 13 predicted hydroxycinnamoyl transferase-encoding genes, mostly with unconfirmed activity and substrates (Schnable *et al.*, 2009). These predicted gene models are candidates for elucidation of the biosynthetic pathway of acetylated feruloylsucroses in maize. Compared to the feruloyl esterification enzymes, the identities of the acetyltransferases that catalyze the acetylation on the glucose ring are less clear. We speculate that these enzymes probably belong to the diverse BAHD acyltransferase family, similar to the acylsugar acyltransferases found in tomatoes (Kim *et al.*, 2012; Schilmiller *et al.*, 2012). Our results lead to the prediction that one or more of these acyltransferases would be positively regulated by ethylene signaling in maize seedling roots. The exact order of feruloyl esterification and acetylation on the sucrose molecule also remains unclear. In rice, nonacetylated 3,6 diferuloylsucrose is detected at a very low concentration in bulk root extract, suggesting that the acetylation occurs after feruloyl esterification (Cho *et al.*, 2015). However, we did not detect the same compound in our microliter-scale LC-MS analyses of maize roots.

Finally, this study has demonstrated the feasibility of combining metabolomics, transcriptomics and quantitative genetics methods to elucidate regulation of previously unknown antifungal metabolites in maize. An expansion of this integrative approach to a larger number of maize inbred lines in a genome-wide association study likely will identify both additional metabolites and genes involved in their metabolism. Such genes will be useful in future breeding efforts to enhance the pathogen resistance during maize seedling establishment.

Acknowledgements

This research was funded by US National Science Foundation awards to 1339237 GJ and 1139329 to GJ and EAS, and US National Science Foundation Graduate Research Fellowship Program award DGE-1650441 to KAK. ESB is funded by the United States Department of Agriculture – Agricultural Research Service. We thank Chong Huang for help with the linear discrimination analysis, Eric Craft and Jon Schaff for help with the RootReader 2D platform, Francis Trail and Robert Procter for sharing the *F. graminearum* ZTE strain, Navid Mohaved for assistance with mass spectrometry, Julia Vrebalov for assistance with ethylene measurement, Eli Borrego for his assistance in ergosterol analyses, and Annett Richter and Melkamu Woldemariam for helpful discussions.

Author contributions

SZ and GJ designed experiments, performed or assisted in all experiments, and wrote the manuscript; KAK and ESB prepared the QuantSeq 3′ mRNA-Seq libraries; YKZ and FCS purified metabolites and performed NMR spectroscopy analyses; JSBae, DKK and HHA assisted in the root imaging experiment, the *Zmacs2-1 Zmacs6* mutant analyses and NIL analyses, respectively; and EAS, YD, MVK and JSBennett conducted fungal infections and *Zmacs2-1 Zmacs6* experiments.

ORCID

John S. Bennett http://orcid.org/0000-0002-7166-9030
Edward S. Buckler http://orcid.org/0000-0002-3100-371X
Georg Jander http://orcid.org/0000-0002-9675-934X
Eric A. Schmelz http://orcid.org/0000-0002-2837-734X
Frank C. Schroeder http://orcid.org/0000-0002-4420-0237
Shaoqun Zhou http://orcid.org/0000-0002-3643-7875

References

Ali ML, Taylor JH, Jie L, Sun G, William M, Kasha KJ, Reid LM, Pauls KP. 2005. Molecular mapping of QTLs for resistance to *Gibberella* ear rot, in corn, caused by *Fusarium graminearum*. *Genome* **48**: 521–533.

Anders S, Pyl PT, Huber W. 2015. Htseq: a python framework to work with high-throughput sequencing data. *Bioinformatics* **31**: 166–169.

Balmer D, de Papajewski DV, Planchamp C, Glauser G, Mauch-Mani B. 2013. Induced resistance in maize is based on organ-specific defence responses. *Plant Journal* **74**: 213–225.

Benson JM, Poland JA, Benson BM, Stromberg EL, Nelson RJ. 2015. Resistance to gray leaf spot of maize: genetic architecture and mechanisms elucidated through nested association mapping and near-isogenic line analysis. *PLoS Genetics* **11**: e1005045.

Benton HP, Want EJ, Ebbels TMD. 2010. Correction of mass calibration gaps in liquid chromatography-mass spectrometry metabolomics data. *Bioinformatics* **26**: 2488–2489.

Bollina V, Kumaraswamy GK, Kushalappa AC, Choo TM, Dion Y, Rioux S, Faubert D, Hamzehzarghani H. 2010. Mass spectrometry-based metabolomics application to identify quantitative resistance-related metabolites in barley against fusarium head blight. *Molecular Plant Pathology* **11**: 769–782.

Brauner PC, Melchinger AE, Schrag TA, Utz HF, Schipprack W, Kessel B, Ouzunova M, Miedaner T. 2017. Low validation rate of quantitative trait loci for gibberella ear rot resistance in european maize. *Theoretical and Applied Genetics* **130**: 175–186.

Buckler ES, Gaut BS, McMullen MD. 2006. Molecular and functional diversity of maize. *Current Opinion in Plant Biology* **9**: 172–176.

Chen T, Li JX, Xu Q. 2000. Phenylpropanoid glycosides from *smilax glabra*. *Phytochemistry* **53**: 1051–1055.

Chen W, Gao Y, Xie W, Gong L, Lu K, Wang W, Li Y, Liu X, Zhang H, Dong H *et al.* 2014. Genome-wide association analyses provide genetic and biochemical insights into natural variation in rice metabolism. *Nature Genetics* **46**: 714–721.

Chen X, Steed A, Travella S, Keller B, Nicholson P. 2009. *Fusarium graminearum* exploits ethylene signalling to colonize dicotyledonous and monocotyledonous plants. *New Phytologist* **182**: 975–983.

Cho JG, Cha BJ, Seo WD, Jeong RH, Shrestha S, Kim JY, Kang HC, Baek NI. 2015. Feruloyl sucrose esters from *Oryza sativa* roots and their tyrosinase inhibition activity. *Chemistry of Natural Compounds* **51**: 1094–1098.

Christensen SA, Nemchenko A, Park YS, Borrego E, Huang PC, Schmelz EA, Kunze S, Feussner I, Yalpani N, Meeley R *et al.* 2014. The novel monocot-specific 9-lipoxygenase zmlox12 is required to mount an effective jasmonate-mediated defense against *Fusarium verticillioides* in maize. *Molecular Plant-Microbe Interactions* **27**: 1263–1276.

Cuomo CA, Gueldener U, Xu JR, Trail F, Turgeon BG, Di Pietro A, Walton JD, Ma LJ, Baker SE, Rep M *et al.* 2007. The *Fusarium graminearum* genome reveals a link between localized polymorphism and pathogen specialization. *Science* **317**: 1400–1402.

Ding LN, Xu HB, Yi HY, Yang LM, Kong ZX, Zhang LX, Xue SL, Jia HY, Ma ZQ. 2011. Resistance to hemi-biotrophic *F. graminearum* infection is associated with coordinated and ordered expression of diverse defense signaling pathways. *PLoS ONE* **6**: e19008.

Ding Y, Huffaker A, Kollner TG, Weckwerth P, Robert CAM, Spencer JL, Lipka AE, Schmelz EA. 2017. Selinene volatiles are essential precursors for maize defense promoting fungal pathogen resistance. *Plant Physiology* **175**: 1455–1468.

Dobin A, Davis CA, Schlesinger F, Drenkow J, Zaleski C, Jha S, Batut P, Chaisson M, Gingeras TR. 2013. Star: ultrafast universal rna-seq aligner. *Bioinformatics* **29**: 15–21.

Eichten SR, Foerster JM, de Leon N, Kai Y, Yeh CT, Liu S, Jeddeloh JA, Schnable PS, Kaeppler SM, Springer NM. 2011. B73-Mo17 near-isogenic lines demonstrate dispersed structural variation in maize. *Plant Physiology* **156**: 1679–1690.

Famoso AN, Clark RT, Shaff JE, Craft E, McCouch SR, Kochian LV. 2010. Development of a novel aluminum tolerance phenotyping platform used for comparisons of cereal aluminum tolerance and investigations into rice aluminum tolerance mechanisms. *Plant Physiology* **153**: 1678–1691.

Gallie DR, Young TE. 2004. The ethylene biosynthetic and perception machinery is differentially expressed during endosperm and embryo development in maize. *Molecular Genetics and Genomics* **271**: 267–281.

Guenther JC, Trail F. 2005. The development and differentiation of *Gibberella zeae* (anamorph: *Fusarium graminearum*) during colonization of wheat. *Mycologia* **97**: 229–237.

Handrick V, Robert CAM, Ahern KR, Zhou SQ, Machado RAR, Maag D, Glauser G, Fernandez-Penny FE, Chandran JN, Rodgers-Melnik E *et al.* 2016. Biosynthesis of 8-o-methylated benzoxazinoid defense compounds in maize. *Plant Cell* **28**: 1682–1700.

Huffaker A, Kaplan F, Vaughan MM, Dafoe NJ, Ni XZ, Rocca JR, Alborn HT, Teal PEA, Schmelz EA. 2011. Novel acidic sesquiterpenoids constitute a dominant class of pathogen-induced phytoalexins in maize. *Plant Physiology* **156**: 2082–2097.

Jiao Y, Peluso P, Shi J, Liang T, Stitzer MC, Wang B, Campbell MS, Stein JC, Wei X, Chin CS *et al.* 2017. Improved maize reference genome with single-molecule technologies. *Nature* **546**: 524–527.

Kazan K, Gardiner DM, Manners JM. 2012. On the trail of a cereal killer: recent advances in *Fusarium graminearum* pathogenomics and host resistance. *Molecular Plant Pathology* **13**: 399–413.

Kebede AZ, Woldemariam T, Reid LM, Harris LJ. 2016. Quantitative trait loci mapping for gibberella ear rot resistance and associated agronomic traits using genotyping-by-sequencing in maize. *Theoretical and Applied Genetics* **129**: 17–29.

Kim J, Kang K, Gonzales-Vigil E, Shi F, Jones AD, Barry CS, Last RL. 2012. Striking natural diversity in glandular trichome acylsugar composition is shaped by variation at the Acyltransferase2 locus in the wild tomato *Solanum habrochaites*. *Plant Physiology* **160**: 1854–1870.

Kim KH, Chang SW, Lee KR. 2010. Feruloyl sucrose derivatives from *Bistorta manshuriensis*. *Canadian Journal of Chemistry-Revue Canadienne De Chimie* **88**: 519–523.

Kremling KAG, Chen SY, Su MH, Lepak NK, Romay MC, Swarts KL, Lu F, Lorant A, Bradbury PJ, Buckler ES. 2018. Dysregulation of expression correlates with rare-allele burden and fitness loss in maize. *Nature* **555**: 520–523.

Kubicek CP, Starr TL, Glass NL. 2014. Plant cell wall-degrading enzymes and their secretion in plant-pathogenic fungi. *Annual Review of Phytopathology* **52**: 427–451.

Kuhl C, Tautenhahn R, Bottcher C, Larson TR, Neumann S. 2012. Camera: an integrated strategy for compound spectra extraction and annotation of liquid chromatography/mass spectrometry data sets. *Analytical Chemistry* **84**: 283–289.

Kuo YH, Hsu YW, Liaw CC, Lee JK, Huang HC, Kuo LMY. 2005. Cytotoxic phenylpropanoid glycosides from the stems of *Smilax china*. *Journal of Natural Products* **68**: 1475–1478.

Lee M, Sharopova N, Beavis WD, Grant D, Katt M, Blair D, Hallauer A. 2002. Expanding the genetic map of maize with the intermated b73 x mo17 (ibm) population. *Plant Molecular Biology* **48**: 453–461.

Li GL, Yen Y. 2008. Jasmonate and ethylene signaling pathway may mediate *Fusarium* head blight resistance in wheat. *Crop Science* **48**: 1888–1896.

Lou YR, Bor M, Yan J, Preuss AS, Jander G. 2016. Arabidopsis NATA1 acetylates putrescine and decreases defense-related hydrogen peroxide accumulation. *Plant Physiology* **171**: 1443–1455.

McMullen MD, Kresovich S, Villeda HS, Bradbury P, Li H, Sun Q, Flint-Garcia S, Thornsberry J, Acharya C, Bottoms C *et al.* 2009. Genetic properties of the maize nested association mapping population. *Science* **325**: 737–740.

Meihls LN, Handrick V, Glauser G, Barbier H, Kaur H, Haribal MM, Lipka AE, Gershenzon J, Buckler ES, Erb M *et al.* 2013. Natural variation in maize aphid resistance is associated with 2,4-dihydroxy-7-methoxy-1,4-benzoxazin-3-one glucoside methyltransferase activity. *Plant Cell* **25**: 2341–2355.

Mideros SX, Windham GL, Williams WP, Nelson RJ. 2012. Tissue-specific components of resistance to aspergillus ear rot of maize. *Phytopathology* **102**: 787–793.

Mueller D. 2016a. *Corn disease loss estimates from the United States and Ontario, Canada – 2013. Purdue University Extension.* [WWW document] URL http://cropprotectionnetwork.org/crop-loss-estimates/corn-disease-loss-estimates-2013/. CPN-2007-13-W [accessed 21 October 2018].

Mueller D. 2016b. *Corn disease loss estimates from the United States and Ontario, Canada - 2014. Purdue University Extension.* [WWW document] URL http://cropprotectionnetwork.org/crop-loss-estimates/corn-disease-loss-estimates-2014/. CPN-2007-14-W [accessed 21 October 2018].

Mueller D. 2017. *Corn disease loss estimates from the United States and Ontario, Canada - 2016. Purdue University Extension.* [WWW document] URL https://cropprotectionnetwork.org/download/5126/ . CPN-2007-16-W. [accessed 21 October 2018].

Munkvold GP, White DG. 2016. *Compendium of corn diseases: the American Phytopathological Society.* St. Paul, MN, USA: The American Phytopathological Society.

Nicholson RL, Hammerschmidt R. 1992. Phenolic-compounds and their role in disease resistance. *Annual Review of Phytopathology* **30**: 369–389.

Olukolu BA, Wang GF, Vontimitta V, Venkata BP, Marla S, Ji J, Gachomo E, Chu K, Negeri A, Benson J *et al.* 2014. A genome-wide association study of the maize hypersensitive defense response identifies genes that cluster in related pathways. *PLoS Genetics* **10**: e1004562.

Ono M, Takamura C, Sugita F, Masuoka C, Yoshimitsu H, Ikeda T, Nohara T. 2007. Two new steroid glycosides and a new sesquiterpenoid glycoside from the underground parts of *Trillium kamtschaticum*. *Chemical & Pharmaceutical Bulletin* **55**: 551–556.

Panda P, Appalashetti M, Natarajan M, Chan-Park MB, Venkatraman SS, Judeh ZM. 2012a. Synthesis and antitumor activity of lapathoside d and its analogs. *European Journal of Medicinal Chemistry* **53**: 1–12.

Panda P, Appalashetti M, Natarajan M, Mary CP, Venkatraman SS, Judeh ZM. 2012b. Synthesis and antiproliferative activity of helonioside a, 3′,4′,6′-tri-o-feruloylsucrose, lapathoside c and their analogs. *European Journal of Medicinal Chemistry* **58**: 418–430.

Pasquet JC, Chaouch S, Macadre C, Balzergue S, Huguet S, Martin-Magniette ML, Bellvert F, Deguercy X, Thareau V, Heintz D *et al.* 2014. Differential gene expression and metabolomic analyses of *Brachypodium distachyon* infected by deoxynivalenol producing and non-producing strains of *Fusarium graminearum*. *BMC Genomics* **15**: 629.

Ponts N, Pinson-Gadais L, Boutigny AL, Barreau C, Richard-Forget F. 2011. Cinnamic-derived acids significantly affect *Fusarium graminearum* growth and *in vitro* synthesis of type b trichothecenes. *Phytopathology* **101**: 929–934.

Proctor RH, Hohn TM, Mccormick SP. 1995. Reduced virulence of *gibberella zeae* caused by disruption of a trichothecene toxin biosynthetic gene. *Molecular Plant–Microbe Interactions* **8**: 593–601.

Schilmiller AL, Charbonneau AL, Last RL. 2012. Identification of a bahd acetyltransferase that produces protective acyl sugars in tomato trichomes. *Proceedings of the National Academy of Sciences, USA* **109**: 16 377–16 382.

Schmelz EA, Kaplan F, Huffaker A, Dafoe NJ, Vaughan MM, Ni XZ, Rocca JR, Alborn HT, Teal PE. 2011. Identity, regulation, and activity of inducible diterpenoid phytoalexins in maize. *Proceedings of the National Academy of Sciences, USA* **108**: 5455–5460.

Schnable PS, Ware D, Fulton RS, Stein JC, Wei F, Pasternak S, Liang C, Zhang J, Fulton L, Graves TA *et al.* 2009. The b73 maize genome: complexity, diversity, and dynamics. *Science* **326**: 1112–1115.

Tautenhahn R, Bottcher C, Neumann S. 2008. Highly sensitive feature detection for high resolution LC/MS. *BMC Bioinformatics* **9**: 504.

Vanden Wymelenberg AJ, Cullen D, Spear RN, Schoenike B, Andrews JH. 1997. Expression of green fluorescent protein in *Aureobasidium pullulans* and quantification of the fungus on leaf surfaces. *BioTechniques* **23**: 686–690.

Wang S, Basten CJ, Zeng Z-B 2012. *Windows qtl cartographer 2.5.* Raleigh, NC: Department of Statistics, North Carolina State University.

Xiao J, Jin XH, Jia XP, Wang HY, Cao AZ, Zhao WP, Pei HY, Xue ZK, He LQ, Chen QG *et al.* 2013. Transcriptome-based discovery of pathways and genes related to resistance against *Fusarium* head blight in wheat landrace Wangshuibai. *BMC Genomics* **14**: 197.

Yan J, Aboshi T, Teraishi M, Strickler SR, Spindel JE, Tung CW, Takata R, Matsumoto F, Maesaka Y, McCouch SR *et al.* 2015. The tyrosine aminomutase tam1 is required for beta-tyrosine biosynthesis in rice. *Plant Cell* **27**: 1265–1278.

Yan L, Gao W, Zhang Y, Wang Y. 2008. A new phenylpropanoid glycosides from *Paris polyphylla* var. *yunnanensis*. *Fitoterapia* **79**: 306–307.

Yang C, Lu X, Ma B, Chen S-Y, Zhang J-S. 2015. Ethylene signaling in rice and *Arabidopsis*: conserved and diverged aspects. *Molecular Plant* **8**: 495–505.

Yang Q, He Y, Kabahuma M, Chaya T, Kelly A, Borrego E, Bian Y, El Kasmi F, Yang L, Teixeira P *et al.* 2017. A gene encoding maize caffeoyl-coa o-methyltransferase confers quantitative resistance to multiple pathogens. *Nature Genetics* **49**: 1364–1372.

Ye JR, Guo YL, Zhang DF, Zhang N, Wang C, Xu ML. 2013. Cytological and molecular characterization of quantitative trait locus *qrfg1*, which confers resistance to gibberella stalk rot in maize. *Molecular Plant–Microbe Interactions* **26**: 1417–1428.

Young TE, Meeley RB, Gallie DR. 2004. Acc synthase expression regulates leaf performance and drought tolerance in maize. *Plant Journal* **40**: 813–825.

Zhang L, Liao CC, Huang HC, Shen YC, Yang LM, Kuo YH. 2008. Antioxidant phenylpropanoid glycosides from *Smilax bracteata*. *Phytochemistry* **69**: 1398–1404.

Zhang Y, He J, Jia LJ, Yuan TL, Zhang D, Guo Y, Wang YF, Tang WH. 2016. Cellular tracking and gene profiling of *Fusarium graminearum* during maize stalk rot disease development elucidates its strategies in confronting phosphorus limitation in the host apoplast. *PLoS Pathogens* **12**: e1005485.

Zhou S, Bae JS, Bergstrom GC, Jander G. 2018. *Fusarium graminearum*-induced shoot elongation and root reduction in maize seedlings correlate with later seedling blight severity. *Plant Direct* **2**: e00075.

Zhu JJ, Zhang CF, Zhang M, Wang ZT. 2006. Studies on chemical constituents in roots of *rumex dentatus*. *Zhongguo Zhong Yao Za Zhi* **31**: 1691–1693.

Supporting Information

Additional supporting information may be found online in the Supporting Information section at the end of the article.

Fig. S1 Natural variation in *Fusarium graminearum*-induced root growth reduction in maize seedlings.

Fig. S2 Predicted feruloylsucrose compounds have characteristic phenylpropanoid-like ultraviolet absorbance profiles.

Fig. S3 Tandem MS spectra of putative acetylated feruloylsucroses.

Fig. S4 Standard curve of smiglaside C.

Fig. S5 QTL mapping of the smilaside A : smiglaside C ratio identifies the same locus on Chromosome 3.

Fig. S6 Constitutive abundance of smilaside A and smiglaside C vary across B73-Mo17 near-isogenic lines.

Fig. S7 Endogenous ethylene production in root is depleted in the *Zmacs2-1 Zmacs6* double mutant maize seedlings.

Fig. S8 1-ACC and 1-MCP treatment has opposite effects on maize seedling height.

Fig. S9 1-ACC and 1-MCP are not directly toxic to *Fusarium graminearum*.

Table S1 List of mass features significantly different between B73 and Mo17 seedling roots constitutively.

Table S2 List of mass features significantly different between mock- and *Fusarium graminearum*-inoculated B73 seedling roots.

Table S3 List of mass features both significantly different between B73 and Mo17 seedling roots constitutively, and responsive to *Fusarium graminearum* inoculation in B73.

Table S4 Chemical shifts and major coupling constants from NMR spectroscopy analysis of smiglaside C.

Table S5 Natural variation in constitutive smilaside A and smiglaside C abundance across intermated B73 × Mo17 recombinant inbred lines and the two parental inbred lines.

Table S6 Normalized and filtered transcript count of all B73 Refgen v3 gene models expressed in the intermated B73 × Mo17 recombinant inbred lines and the two parental inbred lines.

Please note: Wiley Blackwell are not responsible for the content or functionality of any Supporting Information supplied by the authors. Any queries (other than missing material) should be directed to the *New Phytologist* Central Office.